

The XMM-Newton view of Plaskett's star and its surroundings ^{*}

N. Linder^{1†}, G. Rauw^{1‡}, A. M. T. Pollock² and I. R. Stevens³

¹*Institut d'Astrophysique et de Géophysique, Université de Liège, Bât. B5c, Allée du 6 Août 17, B-4000 Liège, Belgium*

²*ESA XMM-Newton Science Operations Centre, ESAC, Apartado 50727, 28080 Madrid, Spain*

³*School of Physics & Astronomy, University of Birmingham, Edgbaston, Birmingham B15 2TT, United Kingdom*

ABSTRACT

XMM-Newton data of Plaskett's star (HD 47129) are used in order to analyse its X-ray spectrum and variability and hence to derive further constraints on the wind interaction in this early-type binary (O6 I + O7.5 I) system.

Conventional models fail to provide a consistent fit of the EPIC and RGS spectra. The lines seen in the RGS spectrum have a temperature of maximum emissivity between 0.18 and 1.4 keV. The EPIC and RGS spectra are best fitted by a non-equilibrium model consisting of a bremsstrahlung continuum at 2.2 ± 0.1 keV and a number of independent emission lines. Our tests also suggest that an overabundance in nitrogen by a factor ~ 6 might be indicated to best represent the RGS spectrum.

On the other hand, a short term variability study of the light curves of the system indicates that the X-ray flux of Plaskett's star did not display any significant variability during our observation. This result holds for all time scales investigated here (from a few minutes to about one hour). Combining our XMM-Newton data with ROSAT archival observations, we find however a significant variability on the orbital time scale. If this behaviour is indeed phase-locked, it suggests a minimum in the X-ray flux when the primary star is in front. This might be attributed to an occultation of the colliding wind region by the body of the primary.

Finally, 71 other X-ray sources have been detected in the field around Plaskett's star and most of them have a near-IR counterpart with colours that are consistent with those of slightly reddened main-sequence objects. Actually, a sizeable fraction of the X-ray sources in the EPIC images could be either foreground or background sources with no direct connection to HD 47129.

Key words: stars: early-type – stars: individual (HD 47129) – X-rays: stars.

1 INTRODUCTION

HD 47129, also known as Plaskett's star, is a spectroscopic binary system that is believed to belong to the Mon OB2 association (at a distance of 1.5 kpc).

The first spectrum of the star was obtained in 1921 and allowed Plaskett to assign an O5e spectral type. The spectrum of the fainter component (the secondary) appeared to be similar to the primary's one, but weaker and more diffuse (Plaskett 1922). The lack of photometric eclipses renders the determination of the orbital inclination rather difficult. Plas-

kett estimated the radii of the stars to be 10 and 9 R_{\odot} and their separation to be about 128.5 R_{\odot} . Then the maximum possible inclination would be 73° , leading to masses of at least 86 and 72 M_{\odot} for the primary and secondary respectively, corresponding to the most massive stars in a binary to that time.

The large mass function of HD 47129 prompted Struve to re-observe this star in 1947-1948 (Struve 1948). He noted that observations made at different times could show small differences in the appearance of the spectra, affecting the relative intensities of the lines of different elements. This effect, nowadays called *Struve-Sahade effect*, is also observed in other massive binary systems where spectral lines of the secondary star appear stronger when the star is approaching the observer and weaker when it is receding.

Bagnuolo et al. (1992) analysed IUE data and found a mass ratio $q = 0.847 \pm 0.12$ (the secondary being more massive than the primary). Assuming an inclination of 70° ,

^{*} Based on observations obtained with XMM-Newton, an ESA science mission with instruments and contributions directly funded by ESA Member States and NASA

[†] E-mail: linder@astro.ulg.ac.be (NL), rauw@astro.ulg.ac.be (GR)

[‡] Research Associate FNRS, Belgium

Table 1. Characteristics of Plaskett’s star (Bagnuolo et al. 1992)

	M/M_{\odot}	Spectral type	T_{eff} [K]	$\log L/L_{\odot}$	R/R_{\odot}	$V \sin i$ [km/s]
Primary	42.2	O7.5 I	35,100	5.80	21.5	75
Secondary	51.0	O6 I	38,400	5.57-5.94	13.8-21.1	310

Table 2. Ephemeris of Plaskett’s star (adapted from Stickland 1997) used throughout this paper. T_0 is the time of conjunction when the primary star is in front. We further list the interstellar neutral hydrogen column density along the line of sight (Diplas & Savage 1994)

P [days]	T_0 (HJD - 2 440 000)	e	n_H [cm^{-2}]
14.3966	3967.42	0.0	1.5×10^{21}

the mass of the primary and secondary would then be equal to $42.5 M_{\odot}$, and $51.0 M_{\odot}$ respectively. These authors used a tomographic technique to separate the spectra of the two components of the system and found spectral types of O7.5 I and O6 I for the primary and for the secondary respectively (see Table 1).

Since both components of Plaskett’s star are luminous supergiants, they possess strong stellar winds and the collision of these winds likely produces a high density interaction zone. Wiggs & Gies (1992) showed that a bow shock surrounds the primary and experiences a Coriolis deflection of approximately 50° .

Stickland (1997) also used IUE data to study the Struve-Sahade effect in Plaskett’s star and concluded that gas streams should be responsible for the secondary radial velocities, which had ‘no sense dynamically’. On the other hand, Bagnuolo et al. (1999) failed to find any evidence of a Struve-Sahade effect.

XMM-Newton data of Plaskett’s star are used here in order to analyse its X-ray spectrum and variability and hence to derive further constraints on the wind interaction in this binary system. The paper is organised as follows. Section 2 describes the observations and the data reduction. In section 3, the spectral analysis of the EPIC and RGS data is discussed. Section 4 presents the results of the variability study of Plaskett’s star, on the orbital time scale (ROSAT data) as well as on the time scale of the *XMM-Newton* observations. Finally, section 5 summarizes the results of this study and gives the conclusions.

2 OBSERVATIONS

Two observations of HD 47129 have been made with the *XMM-Newton* satellite (Jansen et al. 2001), the first one on 17th September 2002 and the second one on 16th March 2003. During the first observation, only the RGS instruments were turned on, for a total exposure time of 21939s. On the other hand, the second observation, with a total exposure time of 21621s, was made with the EPIC and RGS instruments turned on. The thick filter was used to reject optical light, and the operating mode was the full window mode for all three EPIC instruments (Turner et al. 2001; Strüder et al. 2001). The two RGS instruments were operated in the de-

fault spectroscopy mode (den Herder et al. 2001) whilst the optical monitor (OM) was turned off because of the brightness of our target.

Version 6.0 of the *XMM-Newton* Science Analysis System (SAS) was used for the data reduction. The EPIC-MOS data were processed through the `emproc` task, while the `epproc` task was used for the EPIC-PN data. Only events with a pattern below 12 (for the MOS instruments) or below 4 (for the PN instrument) were considered. No indication of a significant pile-up was found in the data. On the other hand, our observation was affected by a high background event due to a ‘soft proton’ flare. Based on a light curve for events with energies above 10 keV, we built a list of good time intervals (GTI) corresponding to low background episodes. The soft proton contamination was filtered out from our observation by applying these GTI to our event lists. The remaining exposure time is 14.583 ks, 14.566 ks and 12.130 ks for MOS 1, MOS 2 and PN, respectively. Finally, the out of time events¹ were removed from the PN image.

In order to create an energy coded three colour (RGB) image of the EPIC field (see Fig. 2), three energy bands were defined: the soft ([400:1000] eV), the medium ([1000:2500] eV) and the hard band ([2500:10000] eV). Nine images were then created, one for each of these energy bands and each instrument. For each energy band, the images from the three instruments were combined into a single image that was exposure corrected using a combined exposure map. Some sources in the FOV are very hard, especially the source to the North-West of Plaskett’s star. A few sources emit their maximum flux in the energy range from 0.4 to 1 keV (in red in Fig. 2). However, the majority of the sources, including Plaskett’s star itself, appear in yellow-green and emit most of their flux at intermediate energies. We will discuss the properties of these sources in Sect. 5.

The RGS data were processed with the SAS task `rgsproc`. The filtering of high background intervals was done in a slightly different way than for the EPIC data. Indeed, for the RGS, the light curve is extracted over the entire energy range. The good thresholds were adopted in order to remove the flares without cutting too many good events. Before the rejection of the bad time intervals, the total observation time was equal to 21938s and 21862s, for the observation in 2002 and 2003, respectively. After the application of the GTI (Good Time Interval) tables, the remaining time was:

- (i) in 2002: 16616s for RGS 1 and 16276s for RGS 2,
- (ii) in 2003: 14157s for RGS 1 and 13555s for RGS 2.

¹ Out of time events are events registered during the readout of a CCD and are thus assigned to a wrong position.

[h!]

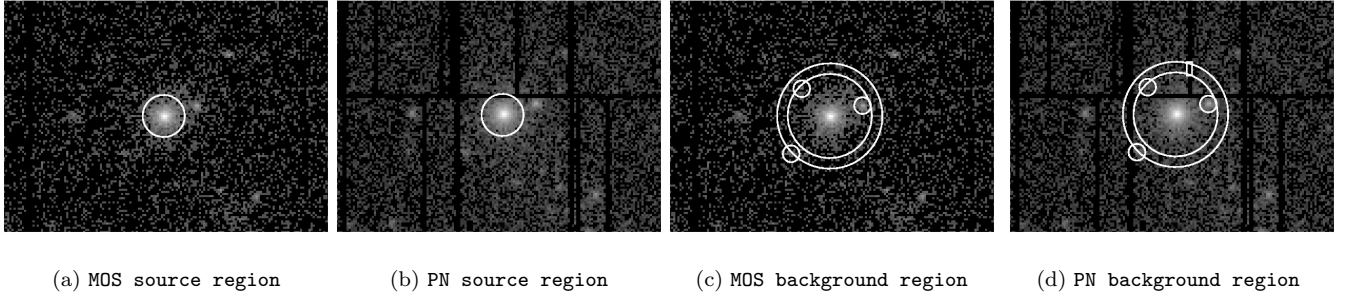


Figure 1. Source and background regions for the MOS and PN instruments (see section 3.1).

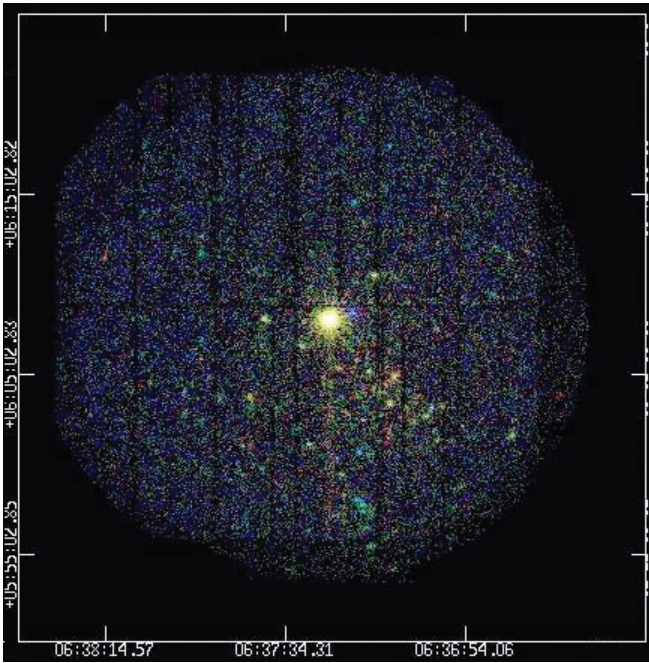


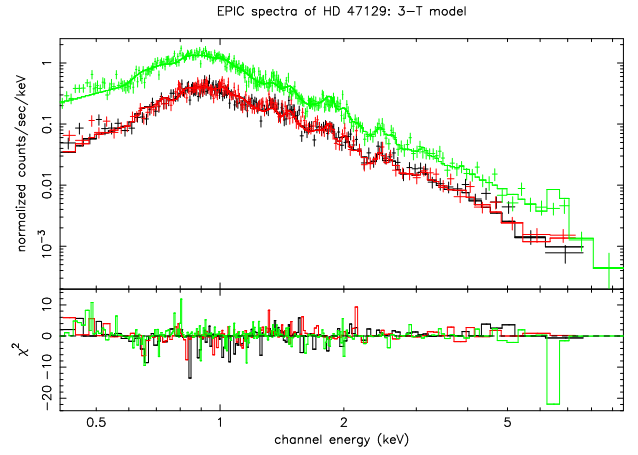
Figure 2. Three colour image of the combined EPIC data. Red = [400:1000] eV, green = [1000:2500] eV and blue = [2500:10000] eV. The North is up and the East is on the left.

3 SPECTRAL ANALYSIS

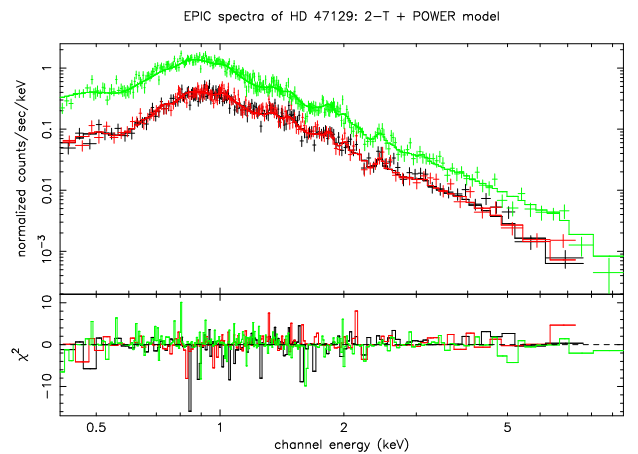
3.1 EPIC spectra

The EPIC spectra were extracted over a circular region of radius 1 arcmin centered on the star including a large part of the Point Spread Function (PSF).

In the case of the MOS instruments, the background spectrum was extracted over an annulus with an inner radius of $r_{min} = 2$ arcmin and $r_{max} = 2.5$ arcmin. However, this annulus also includes three secondary sources that have to be excluded (see Fig. 1(c)). The background region of the PN data is slightly different because a bad column is included in the annulus. This bad column was removed manually from the annulus (see Fig. 1(d)). The Response Matrix Files (RMFs) were generated by the `rmfgen` SAS task and the Ancillary Response Files (ARFs) by the `arfgen` task.



(a)



(b)

Figure 3. EPIC spectra of Plaskett's star from 0.4 keV to 10 keV, fitted with (a) $ISM * [mekal + (wind * mekal) + (wind * mekal)]$ and (b) $ISM * [mekal + (wind * mekal) + (wind * powerlaw)]$ models (see Table 3). MOS 1 is in black, MOS 2 is in red and PN is in green.

The spectra were fitted with various models using the *xspec* software, v11.3.1 (Arnaud 1996). We tested several combinations of absorbed optically thin thermal plasma (*mekal*) and power law models. The choice of these model components is motivated by the fact that the X-ray emission of massive stars can (to first approximation at least, see section 3.4) be represented by an optically thin thermal plasma. The power law component is added to account for a possible inverse Compton tail that could be produced by relativistic electrons accelerated in the wind collision zone. In all test models, the interstellar absorption along the line of sight towards Plaskett's star was frozen at a column density of neutral hydrogen equal to $1.5 \times 10^{21} \text{ cm}^{-2}$ (Diplas & Savage 1994, see Table 2). In addition, two models built to simulate the opacity of the stellar winds have been considered (see Nazé 2004): 'wind1' accounts for the absorption by the stellar wind of the primary star, whilst 'wind2' is designed to simulate absorption by the stellar wind of the secondary. Both wind opacity models turned out to be equivalent in terms of the quality of the spectral fits and in the following, we focus on results obtained with the primary wind model.

In Fig. 3, Plaskett's star spectra are presented, fitted with a model with three temperatures (a), and a model with two temperatures and a power law (b). The comparison between these two figures shows that there is no obvious *K* line of iron in the X-ray spectrum of HD 47129, and for this reason a power law component is apparently more appropriate to represent the high energy tail than a third *mekal* component. The statistically best fit to the EPIC data was achieved for a model $\text{ISM} * [\text{mekal} + (\text{wind} * \text{mekal}) + (\text{wind} * \text{powerlaw})]$.

The softer *mekal* component of this model has a temperature of 0.64 keV, quite typical of the intrinsic X-ray emission of O-type stars. The other *mekal* component has a temperature of 1.25 keV. Although it is higher than expected for shocks intrinsic to the winds, this value is not as extreme as the temperature seen for several other colliding wind binaries (e.g. WR 140 (Pollock et al. 2005), WR 25 (Raassen et al. 2003) and WR 22 (Gosset et al. 2006, in preparation)). Finally, the power law component has a photon index of 2.6. This value is quite large, but is reminiscent of the results obtained for other O-star binaries (e.g. HD 159176, De Becker et al. 2004).

3.2 RGS spectra

The RGS spectra of Plaskett's star at the two epochs are presented in Fig. 4. The main lines have been identified with the line list of the SPEX plasma code (Kaastra et al. 2005): apart from the Fe XVII lines, most features are H or He-like transitions of Si, Mg, Ne, O and N. If we define the zero phase to be the conjunction with the primary star being in front, Φ was equal to 0.10 during the observation of 2002, and equal to 0.63 in 2003. Some differences can be seen between these two observations. First, the nitrogen line at 24.8 Å seems to be stronger in 2002 than in 2003. This could be explained by the fact that the primary star has a stellar wind enriched in nitrogen (see section 3.3 below). Second, the Fe lines are stronger in 2003 than in 2002.

All prominent lines in the RGS spectra have their maximum emissivity occurring at temperatures between 0.18 and 1.4 keV. While the upper temperature limit is quite close to the temperature of the hotter component (1.2 keV) found

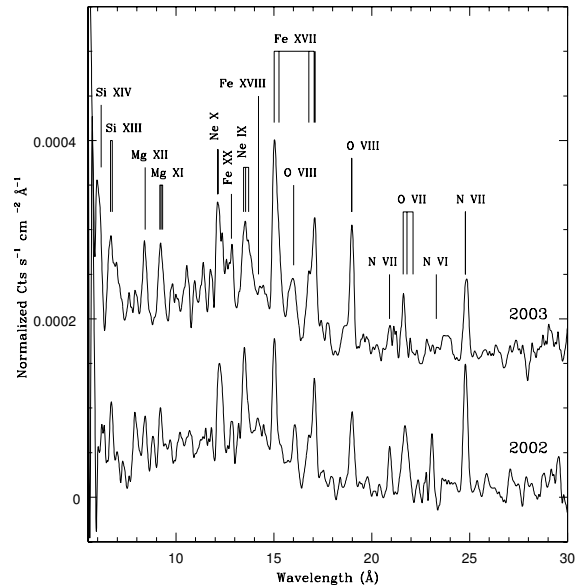


Figure 4. RGS spectra of Plaskett's star, obtained with the rgs-fluxer SAS command (RGS 1 and RGS 2, first and second order). The upper spectrum has been obtained with the data of the 16th of March 2003 ($\Phi = 0.63$), while the lower one is from the data of the 17th of September 2002 ($\Phi = 0.10$). The 2003 spectrum has been shifted upwards by 0.00015.

when fitting a model with two different *mekal* components on the EPIC data, the lower limit is significantly cooler than the softer component (0.6 keV). On the other hand, when a model with three *mekal* components was fitted on the EPIC data, the lower temperature was equal to 0.26 keV, which is much closer to 0.18 keV.

The results of the fits of the RGS data are similar for the two observations (except for the normalisations and hence the fluxes), but are quite different from those obtained with the EPIC data (see Table 3). Because of the low number of photons, χ^2 statistic is not optimal to determine a minimum when fitting. For this reason, the Cash statistic has been used instead of χ^2 . For models with two *mekal* and a powerlaw component, one of the two temperatures is equal to 0.6 keV, while the second one is equal to 0.08 keV, which is the lower limit of the *mekal* models available within *xspec*. The column density affecting all model components also converges towards the lower limit of the *wind* model. The photon index is reduced to about 1.2, whilst its value for EPIC data was equal to 2.6. All models of Tab. 3 have a power law component. The reason is that without such a component, the hottest temperature of the *mekal* components is not well constrained. The value of the flux is slightly larger in 2003 than in 2002 (25 - 30 %). We further note that in 2003 the fluxes deduced from RGS models are about 10 % larger than those obtained from the fits of EPIC spectra.

3.3 Nitrogen overabundance ?

The N VII Ly α line at 24.8 Å is quite prominent in both RGS spectra (see Fig. 4) despite the moderate ISM absorption. In the EPIC spectra, this line produces a bump near 0.5 keV. This prompted us to test also models with a non-

Table 3 (a) Parameters for EPIC spectra of HD 47129. The fits have been performed with *xspec* on the three EPIC spectra simultaneously. (b) Same but for the RGS spectra of HD 47129. The fits have been performed on the first two orders of the RGS spectra, simultaneously. The interstellar absorption is frozen to the value $1.5 \times 10^{21} \text{ cm}^{-2}$ (Diplas & Savage 1994). The two absorption columns in this table represent the absorption by the ionized wind material. Γ is the photon index of the power law component. F is the observed flux and F_c is the flux corrected from the interstellar absorption between 0.4 and 10.0 keV. The error bars represent the 90 % confidence interval.

(a) EPIC DATA

ISM * (mekal ₁ + wind ₂ * mekal ₂ + wind ₃ * mekal ₃)										
(<i>kT</i>) ₁ [keV]	Norm ₁ 10 ⁻³	(<i>nH</i>) ₂ [10 ²¹ cm ⁻²]	(<i>kT</i>) ₂ [keV]	Norm ₂ 10 ⁻³	(<i>nH</i>) ₃ [10 ²¹ cm ⁻²]	(<i>kT</i>) ₃ [keV]	Norm ₃ 10 ⁻³	χ^2 (d.o.f.)	F [erg cm ⁻² s ⁻¹]	F_c [erg cm ⁻² s ⁻¹]
0.31 ^{+0.02} _{-0.01}	0.50 ^{+0.04} _{-0.07}	4.7 ^{+0.6} _{-0.7}	0.74 ^{+0.03} _{-0.02}	1.49 ^{+0.22} _{-0.20}	3.0 ^{+1.3} _{-1.5}	2.42 ^{+0.39} _{-0.16}	1.26 ^{+0.13} _{-0.20}	1.30 (613)	2.60 × 10 ⁻¹²	3.63 × 10 ⁻¹²
ISM * (mekal ₁ + wind ₂ * mekal ₂ + wind ₃ * powerlaw ₃)										
(<i>kT</i>) ₁ [keV]	Norm ₁ 10 ⁻³	(<i>nH</i>) ₂ [10 ²¹ cm ⁻²]	(<i>kT</i>) ₂ [keV]	Norm ₂ 10 ⁻³	(<i>nH</i>) ₃ [10 ²¹ cm ⁻²]	(Γ) ₃	Norm ₃ 10 ⁻³	χ^2 (d.o.f.)	F [erg cm ⁻² s ⁻¹]	F_c [erg cm ⁻² s ⁻¹]
0.64 ^{+0.01} _{-0.02}	0.48 ^{+0.03} _{-0.02}	6.8 ^{+1.3} _{-1.4}	1.24 ^{+0.11} _{-0.16}	0.97 ^{+0.23} _{-0.23}	0.7 ^{+0.6} _{-0.6}	2.56 ^{+0.12} _{-0.14}	0.55 ^{+0.13} _{-0.12}	1.14 (613)	2.65 × 10 ⁻¹²	3.78 × 10 ⁻¹²

(b) RGS DATA

ISM * (mekal ₁ + wind ₂ * powerlaw ₂)										
(<i>kT</i>) ₁ [keV]	Norm ₁ 10 ⁻³	(<i>nH</i>) ₂ [10 ²¹ cm ⁻²]	Γ_2	Norm ₂ 10 ⁻³	C-stat (<i>nbin</i>)	F [erg cm ⁻² s ⁻¹]	F_c [erg cm ⁻² s ⁻¹]			
2002	0.63 ^{+0.03} _{-0.03}	0.33 ^{+0.04} _{-0.04}	0.08 ^{+0.5} _{-0.0}	1.73 ^{+0.15} _{-0.15}	473.76 (321)	2.16 10 ⁻¹²	3.20 10 ⁻¹²			
2003	0.62 ^{+0.03} _{-0.03}	0.47 ^{+0.05} _{-0.05}	0.08 ^{+0.34} _{-0.0}	1.49 ^{+0.15} _{-0.16}	629.72 (357)	2.90 10 ⁻¹²	4.17 10 ⁻¹²			
ISM * (mekal ₁ + wind ₂ * mekal ₂ + wind ₃ * powerlaw ₃)										
(<i>kT</i>) ₁ [keV]	Norm ₁ 10 ⁻³	(<i>nH</i>) ₂ [10 ²¹ cm ⁻²]	(<i>kT</i>) ₂ [keV]	Norm ₂ 10 ⁻³	(<i>nH</i>) ₃ [10 ²¹ cm ⁻²]	Γ_3	Norm ₃ 10 ⁻³	C-stat (<i>nbin</i>)	F [erg cm ⁻² s ⁻¹]	F_c [erg cm ⁻² s ⁻¹]
2002	0.09 ^{+0.03} _{-0.01}	1.68 ^{+2.10} _{-1.10}	0.08 ^{+0.52} _{-0.}	0.40 ^{+0.05} _{-0.05}	0.08 ^{+0.46} _{-0.}	1.20 ^{+0.23} _{-0.28}	0.59 ^{+0.07} _{-0.08}	625.42 (321)	2.33 10 ⁻¹²	3.47 10 ⁻¹²
2003	0.08 ^{+0.02} _{-0.}	1.90 ^{+1.0} _{-1.50}	0.08 ^{+0.61} _{-0.}	0.51 ^{+0.06} _{-0.06}	0.08 ^{+0.34} _{-0.}	1.28 ^{+0.21} _{-0.21}	0.81 ^{+0.09} _{-0.08}	616.63 (357)	2.99 10 ⁻¹²	4.34 10 ⁻¹²

solar nitrogen abundance. When only EPIC data are fitted, no improvement is observed and the nitrogen abundance tends to vanish. Actually, the power law component with a photon index ~ 2.6 seems to account for the bump at 0.5 keV in the EPIC spectra.

On the other hand, for all models tested, when only the RGS data are fitted, the fit yields a nitrogen overabundance (compared to solar abundance) by a factor $7.44^{+4.08}_{-2.59}$ in 2002, and $5.49^{+4.51}_{-2.71}$ in 2003. With its superior spectral resolution, the RGS allows us to confirm that the 0.5 keV feature is actually due to N VII line emission rather than to continuum. This suggests that, if a power law component is indeed present in the X-ray spectrum of HD 47129, it is probably not as steep as indicated by the EPIC fits. We note that no evidence of an oxygen underabundance could be found in the RGS data.

Baguolo & Barry (1996) already noted from optical data that the spectrum of the primary component presents an overabundance in nitrogen, coupled with a depletion in C and O, although they did not provide quantitative results. Furthermore, the secondary component, which is the most massive one, has also a large rotational velocity. Baguolo et al. (1992) accordingly suggested that the primary was initially the most massive star of the system and had transferred mass and angular momentum to the secondary through Roche lobe overflow.

3.4 Consistency of the thermal models

It can be seen from Tab. 3 that the fluxes and model parameters calculated from the EPIC data and from the RGS data are not the same. The reason of this difference could be that the thermal models used (`mekal` models from `xspec`) to fit the data are not appropriate in this case. Indeed, the X-ray emission of plasma is made up of some combination of ionic lines and electron (bremsstrahlung) continuum that are probably excited by shocks (see section 4.1). When ions and electrons are in equilibrium with each other, the X-ray emission produced is properly called thermal emission. However, in the hot plasma in early-type stellar winds, exchanges between ions and electrons are so slow that the X-ray plasma might not be in equilibrium (Pollock & Raassen 2005). Models like `mekal`, which rely on the assumption that there is equilibrium, could thus not be the most useful ones to represent the spectrum of a colliding wind binary such as Plaskett's star.

Instead of the model combinations shown in Tab. 3, we assumed that the continuum can be modelled by isothermal bremsstrahlung subject to interstellar absorption, to which we added 85 delta function lines from N VII (Ly β) to Ar XVIII. Each line was defined by its laboratory wavelength and one or several possible profiles which define a velocity shift and a velocity width. Furthermore, there are no constraints on the intensity of any lines except the intensity ratio of the Lyman series doublets which is fixed at 2:1. Such a model applied to the March 2003 data is shown in Fig. 5. The temperature of the continuum represented by the bremsstrahlung component has been found equal to 2.22 ± 0.1 keV. With this kind of model, there is no need for a power law component at higher energies and both EPIC and RGS data are fitted consistently. The model yields an observed flux of 2.70×10^{-12} erg cm $^{-2}$ s $^{-1}$

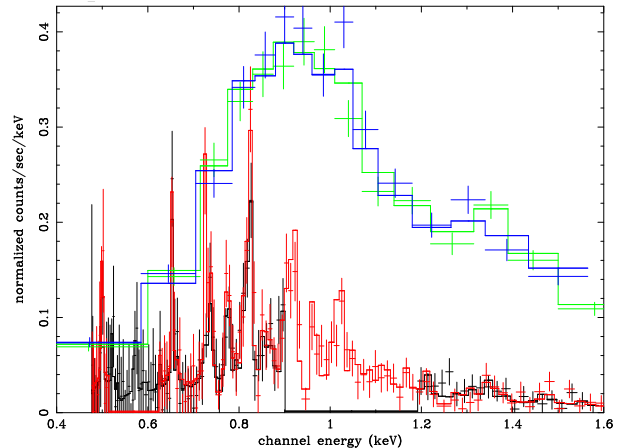


Figure 5. EPIC-MOS and RGS spectra of Plaskett's star as observed in March 2003, from 0.3 to 3 keV, fitted with a bremsstrahlung model and 85 individual lines. This figure appears in colours in the electronic version of the journal, where MOS 1 is in blue, MOS 2 in green, RGS 1 in black and RGS 2 in red.

as well as a flux corrected for interstellar absorption of 3.27×10^{-12} erg cm $^{-2}$ s $^{-1}$.

4 PLASKETT'S STAR AS A COLLIDING WIND BINARY

4.1 X-ray luminosity

The X-ray flux of Plaskett's star in the energy band 0.5 to 10.0 keV, calculated from the model presented in Fig. 5 and corrected for the interstellar absorption, is equal to 3.10×10^{-12} erg cm $^{-2}$ s $^{-1}$. Assuming a distance from Earth of 1500 pc (Berghöfer & Christian 2002), this yields an X-ray luminosity L_X equal to 8.34×10^{32} erg s $^{-1}$.

In Fig. 6(a), L_X/L_{bol} ratios of some O + O binaries observed with XMM-Newton are compared to the empirical scaling relations of Berghöfer et al. (1997) and Sana et al. (2006c). It is often found that O + O and WR + O binary systems display larger L_X/L_{bol} ratios than single stars, and this excess in X-ray emission is usually attributed to colliding wind interactions (Pollock 1987; Chlebowski & Garmany 1991). Berghöfer et al. (1997) did not exclude binary systems from their study, while Sana et al. (2006c) considered only stars without an obvious colliding wind contribution to their X-ray emission. Furthermore, Berghöfer et al. (1997) calculated the X-ray fluxes of their stars between 0.1 and 2.0 keV. It is clear that some of the binary systems of our sample display indeed an excess in X-ray flux.

At this stage, it is worth reviewing the L_X/L_{bol} ratios of a sample of colliding wind O + O binaries that have been observed with XMM-Newton. Fig. 6(a) suggests that the X-ray overluminosity (i.e. the excess in the L_X/L_{bol} ratio as compared to the 'canonical' relation) increases with L_{bol} . This trend could be explained by the general scaling of the mass loss rate \dot{M} with L_{bol} (e.g. Vink et al. 2000) and the fact that the X-ray emission of the wind interaction zone should increase with \dot{M} . Indeed, for an isothermal wind interaction zone, Stevens et al. (1992) predict that $L_X \propto \dot{M} v^2$, whilst

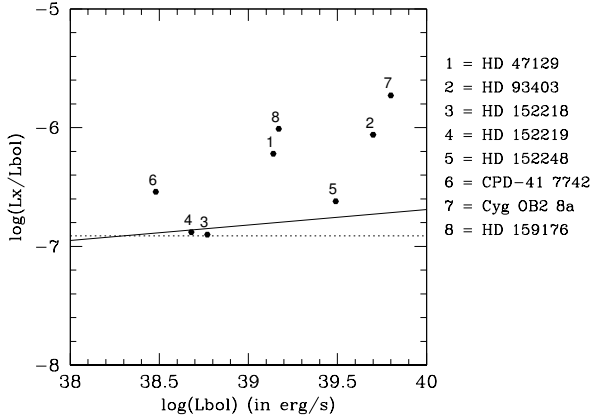
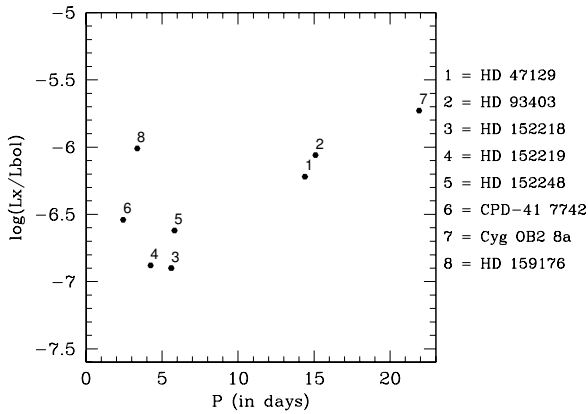

 (a) L_X/L_{bol} vs. bolometric luminosity

 (b) L_X/L_{bol} vs. orbital period

Figure 6. XMM-Newton X-ray luminosities in the energy range 0.5 to 10.0 keV for a sample of massive close O + O binaries. The solid and the dotted lines in the upper panel show the empirical scaling relations derived by Berghöfer et al. (1997) and Sana et al. (2006c), respectively (see section 4.1). Data points for the different objects are from: Rauw et al. 2002b (HD 93403), Sana et al. 2006b (HD 152218), Sana et al. 2006a (HD 152219), Sana et al. 2004 (HD 152248), Sana et al. 2005 (CPD-41°7742), De Becker et al. 2006 (Cyg OB2 # 8a) and De Becker et al. 2004 (HD 159176).

in the adiabatic case $L_X \propto \dot{M}^2 v^{-3.2} d^{-1}$, where L_X , v and d stand for the intrinsic (i.e. unabsorbed by the circumstellar material) X-ray luminosity, the pre-shock velocity and the separation between the stars respectively. We note that there are however exceptions to the general trend of the excess X-ray luminosity with L_{bol} . For instance, HD 152248 displays only a moderate X-ray overluminosity despite its rather large bolometric luminosity, whereas CPD-41° 7742 has a rather large X-ray excess for its bolometric luminosity. In the latter case, we should bear in mind that this system experiences a somewhat peculiar wind interaction since the primary wind actually hits the secondary's photosphere (Sana et al. 2005).

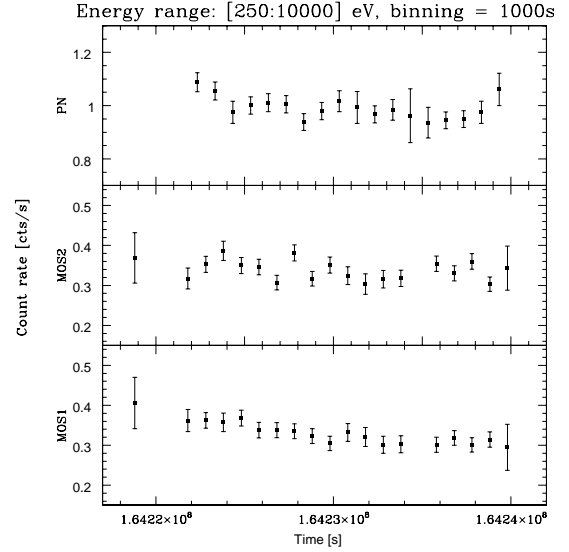


Figure 7. Light curve of Plaskett's star over the duration of our March 2003 XMM-Newton observation, corrected for the background, in the energy band = [250:10000] eV and for a binning of 1000s

Fig. 6(b) displays the L_X/L_{bol} ratio as a function of the orbital period. This plot provides a rough idea of the scaling of the excess X-ray luminosity with orbital separation, suggesting that the excess emission increases when the orbital period increases. This might reflect the dependence of L_X on the pre-shock velocity in the isothermal regime and the fact that in close binary systems with short orbital periods, the winds cannot reach their terminal velocity before they collide. Again, there seems to be an exception to this rule (HD 159176). Finally, we note that for longer orbital periods (i.e. for colliding wind systems in the adiabatic regime), the X-ray excess with respect to the canonical relation should again decrease due to the $1/d$ dependence of L_X .

4.2 Short term variability

Beside the orbital modulation discussed herebelow, the X-ray flux could also be variable on a much shorter timescale due to hydrodynamic instabilities in the colliding wind region (Stevens et al. 1992). In order to look for this variability, we consider the EPIC light curves of our XMM-Newton observation. We searched for a variability on the time scale of our observation, with binnings of 100, 500, 1000 and 4000 seconds, and we considered different energy bands: [250:1000], [1000:2500], [2500:10000] and [250:10000] eV. The count rates were calculated after the application of the GTI tables and the subtraction of the background. No significant variability was apparent on the different light curves (see for example Fig. 7 where the binning is equal to 1000s and the energy range is equal to [250:10000] eV). In order to confirm this result, we applied three different variability tests (χ^2 , Kolmogorov-Smirnov and probability of variability test as described in Sana et al. (2004)). None of these tests detected any consistent significant variability.

Table 4. Journal of the *ROSAT* observations of HD 47129. The sequence numbers starting with rp and rh refer to PSPC and HRI observations respectively.

Obs. seq. number	JD-2440000	CR (10^{-2} cts s $^{-1}$)
rp201265n00	8904.778	11.89 ± 0.58
rh201975n00	9633.452	6.42 ± 0.97
rh201976n00	9633.652	5.80 ± 0.51
rh201977n00	9634.676	5.53 ± 0.40
rh201978n00	9635.670	6.11 ± 0.41
rh201979n00	9636.702	6.34 ± 0.47
rh201980n00	9637.737	5.08 ± 0.51
rh201981n00	9638.631	4.35 ± 0.36
rh201982n00	9639.627	4.50 ± 0.36
rh201983n00	9640.622	3.72 ± 0.32
rh201984n00	9641.618	5.43 ± 0.37
rh201985n00	9642.580	5.12 ± 0.45
rh201972n00	9817.927	5.59 ± 0.39
rh201973n00	9819.477	7.02 ± 0.78
rh201974n00	9820.474	4.41 ± 0.38
rh201975a01	9821.667	4.82 ± 0.42

4.3 ROSAT archival data

The X-ray emission from most colliding wind binaries is expected to display a significant phase-locked variability, either because the opacity changes with the line of sight, and/or because of the changing separation between the stars if the orbit is eccentric. Plaskett’s star has been observed quite extensively with the *ROSAT* satellite allowing us to search for this X-ray modulation.

A *ROSAT*-PSPC (Position Sensitive Proportional Counter) observation of HD 47129 was obtained in 1992 (PI A.W.A. Pauldrach). We have extracted the PSPC spectrum with the `xselect` software over a circular region of radius 1 arcmin. The background spectrum was evaluated over an annulus of outer radius 105 arcsec.

Using `xspec`, we modelled the spectrum by an absorbed single-temperature `mekal` model. Given the rather limited spectral resolution and the small energy domain of the PSPC spectrum, additional model components would not be constrained by the data. The absorption column was modelled by a fixed neutral ISM absorption ($n_{\text{H}} = 1.5 \times 10^{21}$ cm $^{-2}$) and a free ionized wind column (using the `wind1` model discussed above). The best fit ($\chi^2_{\nu} = 1.06$ for 17 degrees of freedom) parameters are $N_w = 10.5^{+1.6}_{-2.1} 10^{21}$ cm $^{-2}$) and $kT = 0.26^{+0.08}_{-0.03}$ keV. The corresponding ISM absorption corrected flux amounts to 2.05×10^{-12} erg cm $^{-2}$ s $^{-1}$ in the 0.5 to 2.5 keV energy range.

In 1994 and 1995, Plaskett’s Star was observed 15 times with the *ROSAT*-HRI (High Resolution Imager, PI T. Berghöfer). These observations provide a rather complete coverage of the orbital cycle, although not with a uniform quality; the durations of the different pointings vary between about 450 and 9000 s. To the best of our knowledge, the results of this campaign were never published. We have analysed these data using the `xselect` software package. Count rates were extracted over a circular source region of radius 20 arcsec centered on Plaskett’s Star, while the background was evaluated over an annulus around the source. The background-corrected HRI count rates are given in Tab. 4 as a function of time.

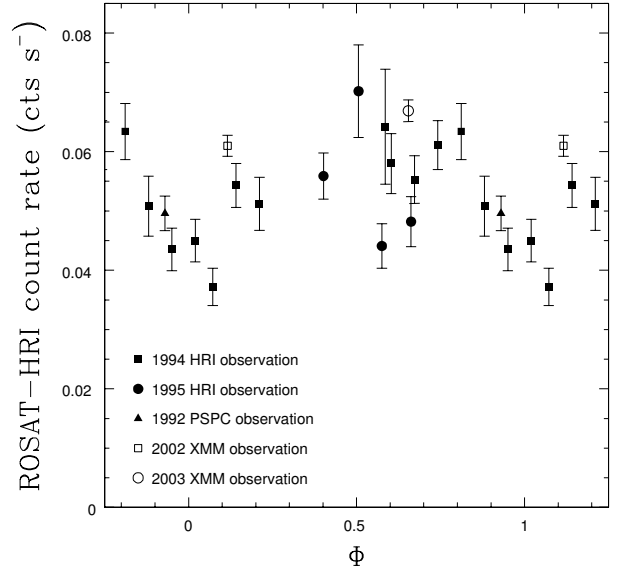


Figure 8. Equivalent HRI count rate as a function of orbital phase evaluated from the ephemeris in Table 2. The filled squares and dots stand for actual HRI observations from 1994 and 1995 respectively. The filled triangle, open square and open dot indicate the equivalent HRI count rate as evaluated by folding respectively the best-fit model for the 1992 PSPC, the 2002 XMM and the 2003 XMM observations through the HRI response matrix.

In Fig. 8, we plot the HRI count rates as a function of the orbital phase using the ephemeris of the *IUE* orbital solution provided by Stickland (1997) where $\Phi = 0$ refers to the time of conjunction when the primary star is in front (see Table 2). There is thus a phase difference of 0.25 between the two conventions. We have folded the best-fit model of the PSPC spectrum discussed above and the best-fit model of the XMM spectra through the HRI response matrix and we thereby evaluate an equivalent HRI count rate. The results are 0.05 ± 0.003 cts s $^{-1}$ for the PSPC (filled triangle in Fig. 8), 0.061 ± 0.002 cts s $^{-1}$ for the first XMM observation (calculated on the RGS data only, the open square in Fig. 8) and 0.067 ± 0.002 cts s $^{-1}$ for the second XMM observation (the open dot in Fig. 8).

Although there is considerable scatter in Fig. 8, we find a roughly sinusoidal modulation of the count rate with a minimum around phase 0. However, a serious problem of Fig. 8 is the apparent discrepancy between the HRI observations of 1994 and 1995. We checked that these discrepant points are not produced by our data analysis by considering the HEASARC archival HRI count rates (High Energy Astrophysics Science Archive Research Center provided by NASA’s Goddard Space Flight Center). The light curve obtained with these archival count rates confirms the results of Fig. 8. Another reason that could possibly explain these variations was the UV sensitivity of the *ROSAT*-HRI detector. Indeed, the instrument was contaminated by the UV band-pass below approximately 4000 Å (Berghöfer et al. 1999). Using the calibration of the HRI UV leak as a function of the U magnitude provided by Berghöfer et al. 1999, we find that in the case of Plaskett’s star ($U=5.227$, Maíz-Apellániz et al. 2004), this contamination induces an error of 1 % on

the count rate, which is not enough to effect the data presented in Fig. 8. The scatter in Fig. 8 does not allow us to conclude that the X-ray variability of Plaskett's star is indeed strictly phase-locked. Still, assuming that the X-ray luminosity undergoes a periodic modulation, we can compare the observed light curve to the model predictions of Pittard & Stevens (1997).

For this purpose, we first derive some general properties of the wind interaction in HD 47129. The wind momentum ratio is defined as:

$$\mathfrak{R} = \left(\frac{\dot{M}_2 v_{\infty 2}}{\dot{M}_1 v_{\infty 1}} \right)^{1/2} \quad (1)$$

where the suffix 1 and 2 indicates the primary and the secondary respectively. \dot{M} is the mass loss rate and v_{∞} the terminal velocity of the wind of the considered star. For HD 47129, reasonable values of \dot{M} are $\sim 5 \times 10^{-7}$ and $\sim 7 \times 10^{-7} M_{\odot} \text{ yr}^{-1}$ for the primary and secondary respectively. These mass loss rates were estimated from the best-fit relation between \dot{M} , L_{bol} and T_{eff} given by Lamers & Leitherer (1993) using the parameters of Table 1. Since the results were larger than the observational determination of the combined $\dot{M} = 1.2 \cdot 10^{-6} M_{\odot} \text{ yr}^{-1}$ (Chlebowski & Garmany 1991), the theoretical mass loss rates were scaled down to fit the observational value. The terminal wind velocities of both stars are most likely quite similar ($\sim 2500 \text{ km s}^{-1}$), leading to $\mathfrak{R} \sim 1.4$. We note that $\mathfrak{R} > 1$ is in agreement with the findings of Wiggs & Gies (1992) that the wind interaction zone should be wrapped around the primary star.

Pittard & Stevens (1997) have calculated hydrodynamic models for three different cases: $\mathfrak{R} = 1$ (Model A), $\mathfrak{R} = 2.2$ (Model B) and $\mathfrak{R} = 5.2$ (Model C). In our case, the situation is intermediate between model A and model B. However, the observed light curve differs from the synthetic curves of model B presented by Pittard & Stevens (1997). In this model, one expects a shallow minimum in the light curve centered on phase 0.5, i.e. at phases when the star with the stronger wind is in front. On the other hand, a maximum occurs in Fig 8 at phase 0.5, when the star with the stronger wind (the secondary) is in front. A possible explanation for this situation could be that the opacity of the primary wind is larger due to the nitrogen enhancement of this wind. This is however at odds with the lack of variability in the wind column density of the circumstellar absorption in Table 3(b). Alternatively, the minimum around $\Phi = 0.0$ could result from the occultation of the X-ray emitting zone of the wind-wind collision by the body of the primary star (in a similar way as the broad occultation seen in CPD-41°7742, Sana et al. 2005). Since the wind collision zone is located closer to the primary star surface, one expects indeed a minimum in the X-ray light curve when the primary is in front. We note however that the rather large Coriolis deflection ($\sim 50^\circ$) inferred by Wiggs & Gies (1992) should produce an occultation of the wind collision zone centered on $\Phi \sim 0.15$ if the maximum X-ray emission arises at the apex of the shock cone. The fact that we observe a minimum centered on $\Phi = 0$ indicates that either the deflection is less than $\sim 50^\circ$, or the maximum X-ray emission does not occur at the shock apex but rather on the part of the shock near the binary axis.

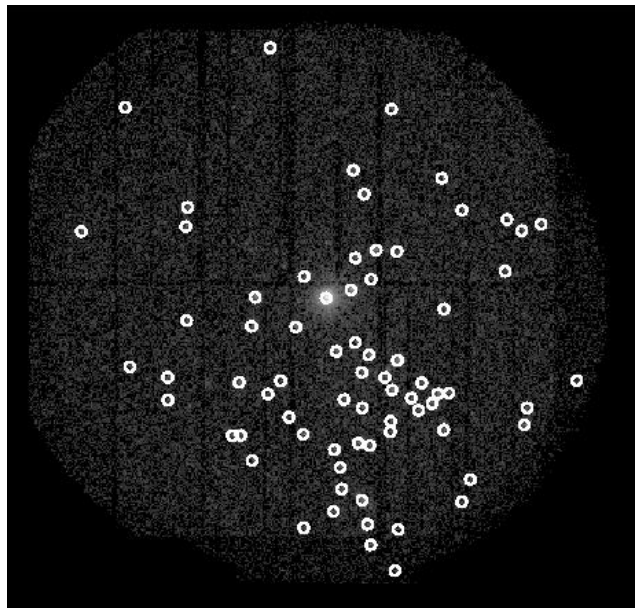


Figure 9. Detection of 71 secondary sources in Plaskett's star field.

5 SECONDARY X-RAY SOURCES

In order to detect secondary X-ray sources in the field of Plaskett's star, we used the SAS task `edetect_chain`. This operation was performed on images with different energy bands ([250:1000], [1000:2500], [2500:10000] eV), and simultaneously on the three EPIC instruments. There are 72 sources (including HD 47129) detected in this way. Their location is presented in Fig. 9.

Among these sources, only a fraction corresponds to known objects and the list of X-ray sources has been compared to existing catalogues in order to determine whether they have a counterpart at other wavelengths. For this purpose, we used three catalogues: the Guide Star Catalogue-II (GSC 2.2 2001), the 2MASS All-Sky Catalog of Point Sources (Cutri et al. 2003) and the US Naval Observatory catalogue (Monet et al. 2003, USNO-B1.0). For each of these catalogues, the correlations were performed with an increasing correlation radius until at least one counterpart was found for each of the 72 sources. The cumulative distribution $\Phi(r)$ of the closest associated counterparts as a function of the cross correlation radius can be approximated as the sum of two terms (see Fig. 10): the cumulative distribution of true correlations, Φ_{true} and the cumulative number of spurious associations Φ_{false} (for details, see Jeffries et al. 1997). This technique is useful to determine the optimal correlation radius, i.e. the correlation radius that yields the maximum number of true correlations (A) while limiting the number of spurious correlations to a minimum. In this way, we find:

- (i) **GSC:** $r_{corr} = 4 \text{ arcsec}$ and $A = 41$;
- (ii) **2MASS:** $r_{corr} = 4 \text{ arcsec}$ and $A = 46$;
- (iii) **USNO:** $r_{corr} = 3.5 \text{ arcsec}$ and $A = 42$.

37 sources have at least one counterpart in each of the three catalogues, and for 32 of them this counterpart is unique. On the other hand, there are 25 sources for which no counterpart could be found in any of the three catalogues.

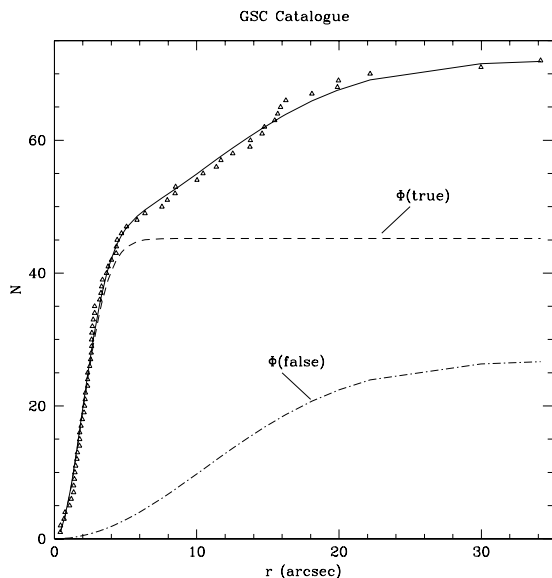


Figure 10. Cumulative distribution (solid line) of the number N of closest associated counterparts as a function of the correlation radius r for the GSC catalogue.

We can obtain a rough estimate of the number of extragalactic (AGN) background sources in our EPIC field of view around HD 47129. The Galactic coordinates of Plaskett’s Star are $l_{\text{II}} = 205.87^\circ$, $b_{\text{II}} = -0.31^\circ$. Although they are in principle not suited for directions at $|b_{\text{II}}| \leq 5^\circ$, we can use the *DIRBE/IRAS* extinction maps provided by Schlegel et al. (1998) to derive a first order estimate of the total Galactic $E(B - V)$ of about 0.72 mag. Given the gas to dust ratio of Bohlin et al. (1978), we thus estimate a neutral hydrogen column density of $\sim 4.2 \times 10^{21} \text{ cm}^{-2}$. Assuming that extragalactic background sources have a power-law spectrum with a photon index of 1.4, and suffer a total interstellar absorption of $4.2 \times 10^{21} \text{ cm}^{-2}$, the detection limit of $3 \times 10^{-3} \text{ cts s}^{-1}$ with the EPIC instruments (pn + MOS1 + MOS2) translates into unabsorbed fluxes of 5.3×10^{-15} and $15.2 \times 10^{-15} \text{ erg cm}^{-2} \text{ s}^{-1}$ in the 0.5 – 2.0 keV and 2.0 – 10 keV band respectively. Using the $\log N - \log S$ relation from Giacconi et al. (2001), one expects thus about 31 – 32 extragalactic objects among the detected X-ray sources.

In a similar way, we can estimate the number of stellar X-ray sources within the field of view around HD 47129. With our detection limit and the $\log N - \log S$ relation for $b_{\text{II}} = 0^\circ$ taken from Motch et al. (2003), we estimate of order 40 stellar X-ray sources (mainly coronal sources and close binaries such as RS CVn systems).

In summary, on statistical grounds a sizeable fraction of the X-ray sources in the EPIC images could be either foreground or background sources. There is no clear excess of X-ray sources that could hint at a population of objects related to HD 47129.

The open cluster NGC 2244, situated in the Rosette Nebula, forms the nucleus of the Mon OB2 association. Plaskett’s star lies at an angular distance of 107 arcmin from the core of the cluster. Assuming that HD 47129 is situated at the same distance from Earth as NGC 2244 (1.5 kpc,

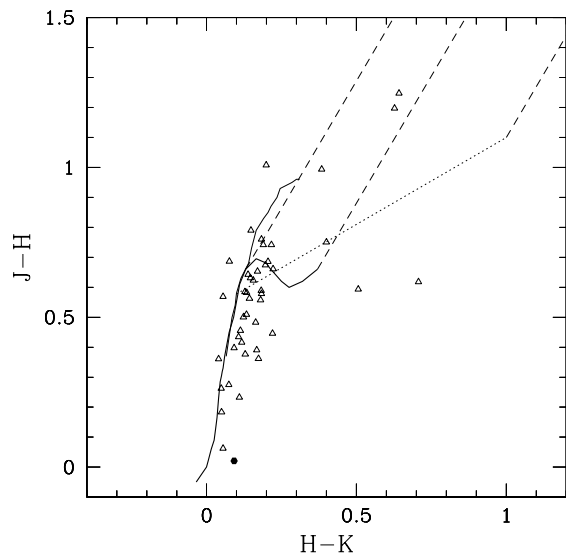


Figure 11. *JHK* colour-colour diagram of the 2MASS counterparts of the X-ray sources in the EPIC field of view around HD 47129. The bold solid line yields the intrinsic near-IR colours of main sequence stars while the other solid line is the locus of unreddened giants. The dotted straight line yields the locus of dereddened colours of classical T Tauri stars (Meyer et al. 1997), whereas the dashed lines form the reddening band for normal dwarf stellar photospheres. Plaskett’s star is indicated by a filled circle.

Berghöfer & Christian 2002), they are separated by at least 46.7 pc, which means that HD 47129 is too far from the cluster to belong to it. Furthermore, the peculiar velocity of the star is rather low, making it unlikely that the binary formed in the cluster and was ejected through subsequent dynamical interactions.

Berghöfer & Christian (2002) found an important number of X-ray bright pre-main sequence stars in NGC 2244. Although HD 47129 is probably not a member of NGC 2244, one could nevertheless expect a priori that a fraction of the X-ray sources near the star might be pre-main sequence objects. In fact, low-mass pre-main sequence stars are commonly associated with massive stars in young open clusters like for instance NGC 6231, NGC 6383 or NGC 6530 (Sana et al. 2006d, Rauw et al. 2002a, Rauw et al. 2003). However, in the present case, there is no clear excess of X-ray sources that could reveal the presence of a sizeable population of low-mass pre-main sequence stars in the surroundings of Plaskett’s star. This fact is confirmed by the $J - H$ vs. $H - K$ diagram derived from the 2MASS data and shown in Fig. 11. Most near-IR counterparts have colours that are consistent with slightly reddened normal stars. The classical T Tauri stars have circumstellar disks that produce an infrared excess and they are thus mostly found towards the right of the reddening band (Meyer et al. 1997). We can see in Fig. 11 that only very few sources of Plaskett’s star field are actually good candidates for classical T Tauri stars, although we cannot rule out that some of the other objects might be weak-line T Tauri stars.

6 SUMMARY AND CONCLUSIONS

In this paper, a study of the X-ray emission of HD 47129 (also called Plaskett's star) has been performed. For this purpose, we analysed two XMM-Newton observations as well as ROSAT archival data.

The EPIC data suggest that the spectrum is best fitted by a two temperature thermal plasma (with $kT_1 = 0.64$ and $kT_2 = 1.25$ keV) and a powerlaw component ($\Gamma \simeq 2.6$). However, the RGS data rather indicate $kT_1 = 0.08$ and $kT_2 = 0.61$ keV with $\Gamma \simeq 1.3$. The different lines seen in the RGS spectrum yield a range of temperatures from 0.18 to 1.4 keV. To solve the discrepancy between the RGS and EPIC fits, we have finally used a model consisting of a bremsstrahlung continuum component along with 85 discrete emission lines. This model allows the electrons to have a different temperature than the ions. Such a situation would not be unexpected in a shock-heated plasma. The best model yields $kT = 2.22 \pm 0.1$ keV for the bremsstrahlung (i.e. the electron) temperature.

The EPIC light curves extracted over different energy bands and with different time bins did not reveal a significant short-term variability on time scales from a few minutes to about one hour. Actually, neither Sana et al. (2004) in the case of HD 152248, nor De Becker et al. (2004) in the case of HD 159176 could find any short-term variability. However, these two binaries were supposed to have more radiative wind interactions than Plaskett's star, and the variability in the X-ray emission should have been stronger than in our case.

We also analysed ROSAT archival data and found a roughly sinusoidal modulation of the count rate. However, the scatter between the data points was too large to allow a deeper analysis.

71 secondary X-ray sources have been detected in the field of view. On statistical grounds, a sizeable fraction of these sources in the EPIC images could be either foreground or background sources. There is no clear excess of X-ray sources compared to the expected number that could indicate the presence of a population of low-mass pre-main sequence stars such as found in very young open clusters.

ACKNOWLEDGMENTS

N. L. acknowledges the financial support of the Belgian "Fonds pour la Formation à la Recherche dans l'Industrie et dans l'Agriculture". This research is supported in part by contract P5/36 IAP (Belspo) and through the XMM/INTEGRAL PRODEX contract.

REFERENCES

Arnaud K. A., 1996, in Jacoby G. H., Barnes J., eds, ASP Conf. Ser. 101: Astronomical Data Analysis Software and Systems V XSPEC: The First Ten Years. p. 17
 Bagnuolo W. G., Gies D. R., Wiggs M. S., 1992, ApJ, 385, 708
 Bagnuolo W. G., Barry D. J., 1996, ApJ, 469, 347
 Bagnuolo W. G., Gies D. R., Riddle R., Penny L. R., 1999, ApJ, 527, 353

Berghöfer T. W., Schmitt J. H. M. M., Danner R., Cassinelli J. P., 1997, A&A, 322, 167
 Berghöfer T. W., Schmitt J. H. M. M., Hünsch M., 1999, A&A, 342, L17
 Berghöfer T. W., Christian D. J., 2002, A&A, 384, 890
 Bohlin R. C., Savage B. D., Drake J. F., 1978, ApJ, 224, 132
 Chlebowski T., Garmany C. D., 1991, ApJ, 368, 241
 Cutri R. M., Skrutskie M. F., Van Dyk S., et al. 2003, University of Massachusetts and Infrared Processing and Analysis Center (IPAC/California Institute of Technology)
 De Becker M., Rauw G., Pittard J. M., Antokhin I. I., Stevens I. R., Gosset E., Owocki S. P., 2004, A&A, 416, 221
 De Becker M., Rauw G., Sana H., Pollock A. M. T., Pittard J. M., Blomme R., Stevens I. R., Van Loo S., 2006, MNRAS, submitted
 den Herder J. W., Brinkman A. C., Kahn S. M., et al. 2001, A&A, 365, L7
 Diplas A., Savage B. D., 1994, ApJS, 93, 211
 Giacconi R., Rosati P., Tozzi P., et al. 2001, ApJ, 551, 624
 GSC 2.2 2001, Space Telescope Science Institute (STScI) and Osservatorio Astronomico di Torino
 Jansen F., Lumb D., Altieri B., et al. 2001, A&A, 365, L1
 Jeffries R. D., Thurston M. R., Pye J. P., 1997, MNRAS, 287, 350
 Kaastra J., Mewe R., Raassen A., 2005, private communication
 Lamers H. J. G. L. M., Leitherer C., 1993, ApJ, 412, 771
 Maíz-Apellániz J., Walborn N. R., Galué H. Á., Wei L. H., 2004, ApJS, 151, 103
 Meyer M. R., Calvet N., Hillenbrand L. A., 1997, AJ, 114, 288
 Monet D. G., Levine S. E., Canzian B., et al. 2003, AJ, 125, 984
 Motch C., Herent O., Guillout P., 2003, Astronomische Nachrichten, 324, 61
 Nazé Y., 2004, PhD Thesis, University of Liège
 Pittard J. M., Stevens I. R., 1997, MNRAS, 292, 298
 Plaskett J. S., 1922, JRASC, 16, 284
 Pollock A. M. T., 1987, ApJ, 320, 283
 Pollock A. M. T., Corcoran M. F., Stevens I. R., Williams P. M., 2005, ApJ, 629, 482
 Pollock A. M. T., Raassen A. A. J., 2005, Proc. JENAM 2005, Massive Stars and High Energy Emission in OB Associations, p. 35
 Raassen A. J. J., van der Hucht K. A., Mewe R., et al. 2003, A&A, 402, 653
 Rauw G., Nazé Y., Gosset E., et al. 2002a, A&A, 395, 499
 Rauw G., Vreux J.-M., Stevens I. R., Gosset E., Sana H., Jamar C., Mason K. O., 2002b, A&A, 388, 552
 Rauw G., De Becker M., Gosset E., Pittard J. M., Stevens I. R., 2003, A&A, 407, 925
 Sana H., Rauw G., Gosset E., 2001, A&A, 370, 121
 Sana H., Stevens I. R., Gosset E., Rauw G., Vreux J.-M., 2004, MNRAS, 350, 809
 Sana H., Antokhina E., Royer P., Manfroid J., Gosset E., Rauw G., Vreux J.-M., 2005, A&A, 441, 213
 Sana H., Gosset E., Rauw G., 2006a, MNRAS, submitted
 Sana H., Nazé Y., O'Donnell B., Rauw G., Gosset E., 2006b, in preparation

- Sana H., Rauw G., Nazé Y., Gosset E., Vreux J.-M., 2006c, MNRAS, submitted
- Sana H., Rauw G., Sung H., Gosset E., Vreux J.-M., 2006d, MNRAS, in preparation
- Schlegel D. J., Finkbeiner D. P., Davis M., 1998, ApJ, 500, 525
- Stevens I. R., Blondin J. M., Pollock A. M. T., 1992, ApJ, 386, 265
- Stickland D. J., 1997, The Observatory, 117, 37
- Strüder L., Briel U., Dennerl K., et al. 2001, A&A, 365, L18
- Struve O., 1948, ApJ, 107, 327
- Turner M. J. L., Abbey A., Arnaud M., et al. 2001, A&A, 365, L27
- Vink J. S., de Koter A., Lamers H. J. G. L. M., 2000, A&A, 362, 295
- Wiggs M. S., Gies D. R., 1992, ApJ, 396, 238